Enhanced Frequency Containment Reserve Provision from Battery Hybridized Hydropower Plants: Theory and Experimental Validation

Francesco Gerini[†], Elena Vagnoni[*], Martin Seydoux[*], Rachid Cherkaoui[†] and Mario Paolone[†]
[†] Distributed Electrical System Laboratory (DESL)
EPFL, Lausanne, Switzerland
[*] Technology Platform for Hydraulic Machines (PTMH)
EPFL, Lausanne, Switzerland

***Abstract*—This paper presents a solution to address wear and tear of *Run-of-River* (RoR) *Hydropower Plants* (HPPs) providing enhanced *Frequency Containment Reserve* (FCR). In this respect, the study proposes the integration of a *Battery Energy Storage System* (BESS) with RoR HPPs controlled by a double-layer *Model Predictive Control* (MPC). The upper layer MPC acts as a state of energy manager for the BESS, employing a forecast of the required regulating energy for the next hour. The lower-layer MPC optimally allocates the power set-point between the turbine and the BESS. Reduced-scale experiments are performed on a one-of-a-kind testing platform to validate the proposed MPC-based control considering a comparison with different control strategies and different BESS sizes. The results demonstrate superior performance of the proposed framework, compared to simpler techniques like dead-band control or to the standalone RoR scenario, leading to improved FCR provision, reduced servomechanism stress, and extended hydropower asset lifespan.**

***Index Terms*—Battery Energy Storage System, Frequency Containment Reserve, Hydropower, Model Predictive Control, Run-of-River Power Plant.**

I. Introduction

As widely recognized, hydropower plants are renewable energy assets that play a crucial role in providing fundamental ancillary grid services, such as *Frequency Containment Reserve* (FCR), which have become increasingly important due to the decommissioning of dispatchable thermal power plants. Part of the FCR reserve is provided by *Run-of-River* (RoR) power plants [1], accounting for 5.94 % of the total generated electricity in the ENTSOE area in 2022 [2].

The need for continuous power regulations impacts the lifetime of hydroelectric assets [3]. RoR *Hydropower Plants* (HPP) are often equipped with double-regulated Kaplan turbines (i.e. machines able to control guide vane and blade opening angles), able to guarantee high-efficiency values through a wide range of water discharge and head conditions. In the case of Kaplan turbines, the lifetime of the servomechanism that controls the movement of the blades is significantly impacted by continuous regulation. Continuous movements can stress the servomechanisms, leading to increased wear and tear, potential mechanical failures, and reduced overall turbine life [4]. To address these challenges, this paper focuses on the hybridization of RoR HPP with *Battery Energy Storage Systems* (BESS) to enhance FCR provision and extend hydropower asset lifetime. This approach has been gathering an increasing interest in the literature [5], [6], [7], [8]. However, despite this interest, many of the existing contributions primarily suggest simple control techniques based on dead-band control or fuzzy logic [7], [5]. Others discuss HPP-BESS hybridization for other applications, such as penstock fatigue reduction in medium-head HPPs [8]. Moreover, most of the above-mentioned contributions are only simulation-based or with very limited experimental validation [6]).

For this reason, the scope of this paper is to propose and experimentally validate an optimal control technique for hybrid RoR HPPs operating under a daily dispatch plan that provide FCR with a fixed droop characteristic. In particular, we present a double-layer *Model Predictive Control* (MPC) to drive the hybrid system. The upper layer MPC (slower and farsighted) ensures the continuous operation of the BESS, by acting as *State of Energy* (SOE) manager, leveraging a forecast of the regulating energy necessary to provide the FCR service in the following hour. The lower layer (faster and short-sighted) is responsible for splitting the requested power set-point between the turbine and the BESS, ensuring the feasible operation of both systems. The framework is validated for different BESS power and energy ratings to study the impact of the BESS sizing on the control problem. Furthermore, the efficacy of the proposed control strategy is examined and validated through reduced-scale experiments conducted on an innovative testing platform [9]. The evaluation covers a comparison with classical control strategies and BESS sizes, with a specific emphasis on assessing the FCR provision quality and the reduction in servomechanism stress.

The paper is organized as follows. Section II proposes the general formulation of the control problem. Section III

This work is funded by the XFLEX HYDRO project. The XFLEX HYDRO project has received funding from the European Union's Horizon 2020 research and innovation programme under grant agreement No 857832.

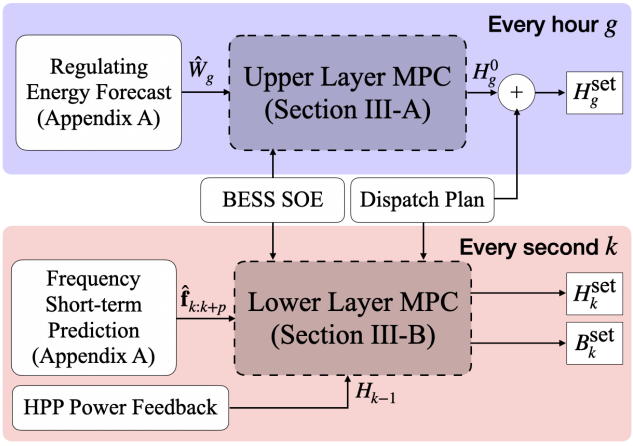

Fig. 1. DLMPC structure, showing inputs and output of the UL (in blue) and LL (in red).

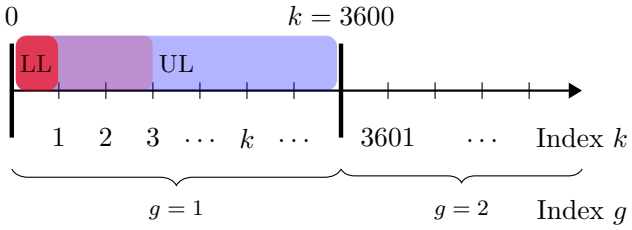

Fig. 2. Timeline of the problem, showing the actuation of the UL in blue, i.e., each hour g, and of the LL in red, i.e., each second k. In light red, the look-ahead horizon of the LL.

presents a detailed description of the two-stage control framework. Section IV provides the experimental validation of the proposed framework. Finally, Section V summarizes the original contributions and main results of the study and proposes perspectives for further research activities.

II. Problem Statement

As stated in Section I, the control addresses run-of-river HPPs operating under daily dispatch plans P^{disp}, scheduled hourly, and obligated to provide FCR service with a fixed droop characteristic[1] σ_f. The dispatch plan, input to the problem, is the product of an external optimization, taking into account market prices and constraints such as the concession head limit and other variables, and not the object of this study. As already stated, a BESS is integrated into the system. The primary focus of this study is to propose an optimal set-point splitting policy that effectively achieves the following objectives:

i) Ensuring dispatch tracking and high-quality FCR provision characterized by a rapid response time, in compliance with stringent FCR requirements [11], [12];
ii) Minimizing the number of movements and the mileage of the hydropower servomechanisms;
iii) Ensuring the continuous and efficient operation of the BESS by managing its SOE within physically feasible limits;
iv) Validating the feasibility of the BESS power set-point to uphold operational constraints composed by the power converter capability curve.

To achieve these objectives, the study proposes the use of a *Double-Layer Model Predictive Control* (DLMPC), structured as visible in Fig. 1. The *upper layer* (UL) acts as a SOE manager for the BESS, employing a forecast of the required regulating energy[2] for each hour g. The output of the UL is a constant power offset for the hour that directly modifies the dispatch plan of the HPP. The *Lower Layer* (LL) optimally allocates the power set point between the turbine and the BESS in real-time, that is, every second k (see the time indices used in Fig. 2). This control layer leverages short-term frequency prediction[3], together with real-time measurement of the HPP power and the BESS SOE. In Fig. 1, each quantity A is indicated with a certain time subscript: hour g or seconds k. In particular, if the quantity is a vector, including information from time k to $k+p$, it is indicated as:

$$\mathbf{A}_{k:k+p} = \left[A_k, A_{k+1}, A_{k+2}, \ldots, A_{k+p-1}, A_{k+p}\right].$$

III. Control Framework

A. Upper Layer MPC

Let us consider H as the power of the hydroelectric unit (active sign notation) and B as the power of BESS (passive sign notation). This MPC layer, executed at the beginning of every hour g, is responsible for computing the smallest constant hourly power offset:

$$H_g^0 = B_g^0$$

that allows to keep the BESS SOE within its physical limits. The problem relies on the last measure of the BESS SOE and a forecast of the frequency integral over the next hour $\hat{W}_g$, together with its confidence intervals $\hat{W}_g^{\uparrow}, \hat{W}_g^{\downarrow}$. Information on the forecasting method can be found in Appendix A. The forecast is modified to take into account the charging efficiency η_{ch} and the discharging efficiency η_{dch} of the BESS as:

$$W_g = \begin{cases} \hat{W}_g \cdot \eta_{\text{ch}}, & \text{if } \hat{W}_g \leq 0 \\ \hat{W}_g / \eta_{\text{dch}}, & \text{if } \hat{W}_g \geq 0 \end{cases} \tag{1}$$

The resulting quantity W_g is the best possible approximation of the energy to provide the FCR service, given a forecast $\hat{W}_f$. However, W_f does not account for the losses related to intra-hour alternating charging/discharging cycles, since an accurate

[1] Numerous European Transmission System Operators (TSOs) source their FCR in a shared market with 4-hour adjustments [10]. However, HPP droop settings tend to remain fixed for extended periods (years or even decades) due to contractual agreements, making them constant inputs in our study.

[2] The idea of forecasting the FCR regulating energy was first introduced by [13] and later used from [14] and others. More information about the way this forecast is performed can be found in Appendix A.

[3] Appendix A examines the viability of this forecast by making references to relevant literature.

FCR power forecast is unavailable. The updated value W_g is an input for the upper layer MPC, where it is used together with the frequency droop σ_f to forecast the regulating energy for hour g for the FCR service:

$$E_g^{\text{FCR}} = \sigma_f \cdot W_g \tag{2}$$

The constant hourly offset B_g^0 is either positive (BESS is charging) or negative (BESS is discharging):

$$B_g^0 = \begin{cases} B_g^{0+} & \text{if charging.} \\ -B_g^{0-} & \text{if discharging.} \end{cases} \tag{3}$$

where B_g^{0+} and B_g^{0-} are the charging and discharging BESS power in kW, respectively. The constant hourly offset B_g^0 is then computed according to the following *Optimisation Problem* (OP):

$$B_g^0 = \underset{B_g^{0+}, B_g^{0-} \in \mathbb{R}}{\arg\min} \left(B_g^{0+} + B_g^{0-}\right)^2 \tag{4a}$$

$$\text{s.t. } W_g = \begin{cases} \hat{W}_g \cdot \eta_{\text{ch}}, & \text{if } \hat{W}_g \leq 0 \\ \hat{W}_g / \eta_{\text{dch}}, & \text{if } \hat{W}_g \geq 0 \end{cases} \tag{4b}$$

$$E_g^{\text{FCR}} = \sigma_f \cdot W_g \tag{4c}$$

$$E_g^0 = \eta_{\text{ch}} \cdot B_g^{0+} - \frac{1}{\eta_{\text{dch}}} \cdot B_g^{0-} \tag{4d}$$

$$SOE_g = SOE_{h-1} + \left[E_g^0 + E_g^{\text{FCR}}\right] \frac{1}{C_{\text{B}}} \tag{4e}$$

$$SOE_g^{\uparrow} = SOE_g + \left[\sigma_f \cdot \hat{W}_g^{\uparrow}\right] \frac{1}{C_{\text{B}}} \tag{4f}$$

$$SOE_g^{\downarrow} = SOE_g - \left[\sigma_f \cdot \hat{W}_g^{\downarrow}\right] \frac{1}{C_{\text{B}}} \tag{4g}$$

$$SOE_g^{\uparrow} \leq SOE_{\max} \tag{4h}$$

$$SOE_g^{\downarrow} \geq SOE_{\min} \tag{4i}$$

$$0 \leq B_g^{0+} \leq B_{\max}^{+} \tag{4j}$$

$$0 \leq B_g^{0-} \leq B_{\max}^{-} \tag{4k}$$

$$B_g^0 = B_g^{+} - B_g^{-} \tag{4l}$$

The energy variation E_g^0 due to the offset action during hour g is provided by Eq. (4d) and expressed in kW h, as the power offset is applied for one hour. The latter is used, together with the forecast of W_g in Eq. (4e) to predict the SOE_g at the end of hour g, taking into consideration the BESS capacity C_{B}. Eqs. (4f)-(4i) compute the confidence interval of the SOE forecast and ensure the feasible operation in the considered intervals.

Separating the charging and discharging components of the power offset allows for taking into consideration charging and discharging efficiency. Relaxation according to [15], visible in Eq. (4a) forces only one of the two decision variables to be different from zero, so that Eq. (4l) is compatible with the definition in Eq. (3). Equations (4j)-(4k) ensure the final power of the battery to be within the operational limits. Finally, Eq. (4l) computes the final power output of the BESS, positive if charging. The offset is directly applied to modify the dispatch plan of the HPP, as visible in Fig. 1.

B. Lower Layer MPC (LLMPC)

The lower layer is a rolling-horizon MPC responsible for computing in real-time (i.e., each second) the set-point splitting policy between the HPP and the BESS, with the following objectives:

a) Optimal tracking of the FCR provision.
b) Minimization the number of movements and the total mileage of the hydropower servomechanisms;
c) BESS operation within its physical limits.

For every time step:

$$k \in [k, k+p],$$

where p is the length of the MPC horizon, the expected power output P_k^{set} of the hybrid system is:

$$P_k^{\text{set}} = P_k^{\text{disp}} + \left[50 - \hat{f}_k\right] \cdot \sigma_f \tag{5}$$

where the term term $\hat{f}_k$ indicates the expected value of the grid frequency at time k. Information about this short-term frequency forecast is contained in Appendix A. As a consequence, the tracking error TE_k is the difference between the expected power output and the actual aggregated production of HPP + BESS, i.e. the power flow at the *Point of Common Coupling* (PCC):

$$\text{TE}_k = P_k^{\text{set}} - \left(H_k - B_k\right) \tag{6}$$

and, over the entire MPC window:

$$\text{TE}_{k:k+p} = \|\mathbf{P}_{k:k+p}^{\text{set}} - \left(\mathbf{H}_{k:k+p} - \mathbf{B}_{k:k+p}\right)\|_2 \tag{7}$$

Eq. (7) models the first objective of the LLMPC, i.e., the optimal tracking of the FCR provision. The second objective, i.e. the reduction of the number of movements of the hydropower actuators, can be modeled as the minimization of the cardinality of the array containing the variation of the hydroelectric unit power output with respect to the previous time instant:

$$\min \quad \text{card}(\mathbf{\Delta H}_{k:k+p}) \tag{8}$$

with $\Delta H_k = H_k - H_{k-1} \quad \forall k \in [k, k+p]$. As discussed in [16], the cardinality of a quantity can be relaxed with its ℓ_1-norm. In other words, $\|\mathbf{\Delta H}_{k:k+p}\|_1$ is the convex envelope of the objective function of Eq. (8). The latter equation can therefore be relaxed, and assumes the following form:

$$\min \quad \gamma \|\mathbf{\Delta H}_{k:k+p}\|_1 \tag{9}$$

where γ is non-negative parameter tuned to achieve the desired sparsity [16]. Equations (7) and (9) constitute the objective of the lower-layer MPC.

The constraints of the OP ensure that the BESS and the HPP operate within their physical limits. In particular, the capability curve ζ of the BESS converter is considered as a function of the voltage on both the DC and AC side (v_k^{DC} and v_k^{AC}, respectively) and of the BESS SOE:

$$B_k \leq \zeta(v_k^{DC}, v_k^{AC}, SOE_k) \tag{10}$$

Similarly to [17], the estimation of the BESS v_k^{DC} is based on the battery Three Time Constant (TTC) model whose dynamic evolution can be expressed as a linear function of battery current by applying the transition matrices ϕ^v,ψ^v,ψ_1^v (see Eq. (12d)). In the TCC model, the quantity x_k is the state vector of the voltage model [4], and the DC current is expressed as i_k^{DC}. The latter is computed in Eq. (12e). The active power at the DC bus B_k^{DC} is related to the active power set-point AC side of the converter B_k^{set} according to (12c). The magnitude of the direct sequence component v_k^{AC} of the phase-to-phase voltage on the AC side of the converter, is assumed to be equal to the last available measurement, as indicated in (12f). Finally, the BESS SOE evolution computed in Eq. (12g) is ensured within its physical limits by Eqs. (12h).

For the HPP, a first-order discrete-time dynamical system is used to model the response H_k to a set point H_k^{set} considering a time constant τ_H:

$$H_k = (1 - \frac{\Delta k}{\tau_H}) \cdot H_{k-1} + \frac{\Delta k}{\tau_H} \cdot H_k^{\text{set}} \tag{11}$$

where Δk is the time interval between two consecutive discrete-time samples (i.e., one second). The HPP output power is limited within $H_{\min}$ and $H_{\max}$ by Eq. (12j) while Eq. (12k) ensures the power ramping rate to be lower than its maximum allowed value $\dot{H}_{\max}$, expressed in $\mathrm{kW\,s^{-1}}$.

The LLMPC, running every second k, is the following OP:

$$\begin{aligned}
&\left[\mathbf{H}_{k:k+p}^{\text{set}}, \mathbf{B}_{k:k+p}^{\text{set}}\right] = \\
&\quad = \underset{\mathbf{H},\mathbf{B}\in\mathbb{R}^p}{\arg\min} \quad \mathrm{TE}_{k:k+p} + \gamma \cdot \|\boldsymbol{\Delta}\mathbf{H}_{k:k+p}\|_1 \qquad (12a)
\end{aligned}$$

subject to:

$$B_k \le \zeta(v_k^{DC}, v_k^{AC}, SOE_k) \tag{12b}$$

$$B_k^{DC} = \begin{cases} B_k^{\text{set}} \cdot \eta_{\text{ch}}, & \forall B_k^{\text{set}} \ge 0 \\ B_k^{\text{set}} / \eta_{\text{dch}}, & \forall B_k^{\text{set}} < 0 \end{cases} \tag{12c}$$

$$v_k^{DC} = \phi_v x_{k-1} + \psi_i^v i_k^{DC} + \psi_1^v \mathbf{1} \tag{12d}$$

$$i_k^{DC} \approx \frac{B_k^{DC}}{v_k^{DC}} \tag{12e}$$

$$v_k^{AC} \approx v_{k-1}^{AC} \tag{12f}$$

$$SOE_k = SOE_{k-1} + i_k^{DC} v_k^{DC} \frac{1}{C_B} \tag{12g}$$

$$SOE_{\min} \le SOE_k \le SOE_{\max} \tag{12h}$$

$$H_k = (1 - \frac{\Delta k}{\tau_H}) \cdot H_{k-1} + \frac{\Delta k}{\tau_H} \cdot H_k^{\text{set}} \tag{12i}$$

$$H_{\min} \le H_k \le H_{\max} \tag{12j}$$

$$-\dot{H}_{\max} \le \Delta H_k \le \dot{H}_{\max} \tag{12k}$$

$$\forall k \in [k, \ldots, k+p]$$

A way to convexify constraints (12b) - (12f) has been presented in [20] and used in [17]. As we assume the dispatch plan to include concession head control and given the short-term horizon of the MPC, no constraints on the concession head are introduced[5]. The OP is solved at each time step k (with updated information) on a sliding horizon from the index k to $k+p$. At each k, the control trajectories for HPP and BESS for the whole residual horizon $\left[\mathbf{H}_{k:k+p}^{\text{set}},\ \mathbf{B}_{k:k+p}^{\text{set}}\right]$ are available. However, only the first components, denoted by: $\left[H_k^{\text{set}}, B_k^{\text{set}}\right]$ are considered for actuation.

IV. Experimental Validation

A. Experimental setup

The hybrid experimental platform used modernizes an existing platform in the *Plateforme Technologique Machines Hydrauliques* (PTMH), at EPFL. The current platform is a closed-loop test rig that allows performance assessments of hydraulic machines in the four-quadrant characteristic curve with an accuracy of 0.2 %, complying with the IEC60193 [22] standard for the testing of reduced scale physical models. The specific hydraulic energy in the closed-loop test rig is generated by two centrifugal pumps. They allow for a maximum head of 100 m and a maximum discharge of 1.4 $\mathrm{m^3 s^{-1}}$. Furthermore, the pressure in the draft tube is set by adjusting the pressure in the downstream reservoir by using a vacuum pump. The hydroelectric unit governing systems is built as a standard speed governor [23] with frequency droop $\sigma_f = 125\,\mathrm{kW\,Hz^{-1}}$ and a dead band of $2\,\mathrm{mHz}$. The choice of droop is dictated by the similarity need with the prototype of the reduced scale model turbine, installed in Vogelgrun (FR) [7], and comprehensively discussed in the Appendix B. The measurement infrastructure employs a distributed sensing system based on *Phasor Measurement Units* (PMUs). This system allows for real-time acquisition of precise power flow data thanks to the PMUs' high reporting rate of 50 frames per second and remarkable accuracy, with a standard deviation equivalent to 0.001 degrees (approximately 18 μrad) and error in the frequency estimation $\le 0.4\,\mathrm{mHz}$ [24]. A 50 kW Kaplan turbine is connected to the grid bus with a synchronous machine, rated 100 kVA. On the same bus, the BESS is connected. For more information about the experimental facility, see [9]. The grid frequency is regulated by a grid emulator, visible in Fig. 4, with a nominal power rating of 100 kVA. The configuration of the hybrid system is illustrated in Figure 3. Since the turbine is connected to the grid through a synchronous machine, a synchro-check mechanism is necessary. The comprehensive list of measurements is detailed in Table I.

B. Experimental Tests

In this section, we present the experimental campaign to validate the proposed framework. A series of 12-hour-long tests are performed under the same grid condition. The frequency time-series enforced at the PCC by the grid emulator

[4]This choice of modeling, based on [18], offers greater accuracy than the commonly used two-time constant model [19]. However, for BESS predictions with a 1-second horizon, simpler models can be utilized, as discussed in Section IV.

[5]In the case of need for modeling constraints on the concession head, similarly to what is done in [21], information about the hill-chart of the runner is needed, to translate power set-points into discharge values.

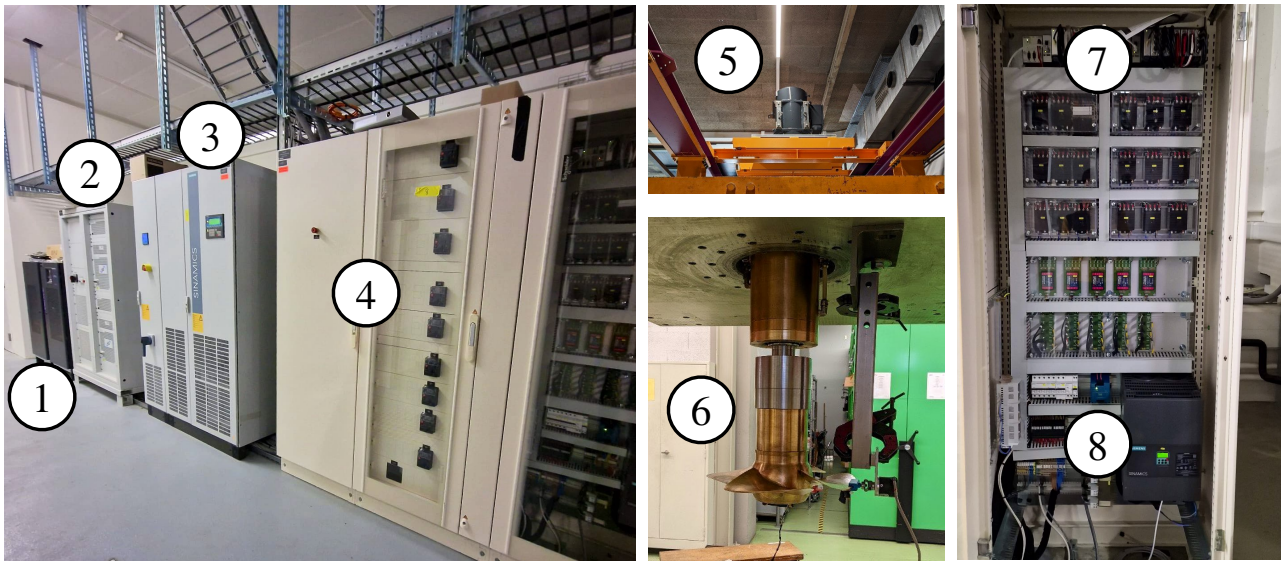

Fig. 3. Photos of the installation in PTMH. 1: BESS converter. 2: Grid emulator. 3: Variable speed converter for the HPP. 4: Automated switches. 5: Synchronous generator. 6: Reduced-scale model of the Kaplan turbine. 7: Measuring system (PMU). 8: Excitation unit.

TABLE I
MEASUREMENTS ON THE PTMH PF3

Hydropower		BESS		PMU	
Name	**Measurement Unit**	**Name**	**Measurement Unit**	**Name**	**Measurement Unit**
Discharge	$\mathrm{m^3\,s^{-1}}$	State of Charge	%	Voltage Magnitude	V
Turbine Speed	rpm	DC Current	A	Voltage Angle	rad
Head	m	DC Power	W	Current Magnitude	A
Hydraulic Efficiency	%	DC Voltage	V	Current Angle	rad
Hydraulic Power	W	Active power	W	Active Power	W
Shaft Torque	N m	Reactive Power	VAr	Reactive Power	VAr
Mechanical Power	W	Temperature	°C	Frequency	Hz
Guide Vanes Opening (GVO)	deg				
Runner Blade Angle (RBA)	deg				
Runner Blade Torque (RBT)	N m				

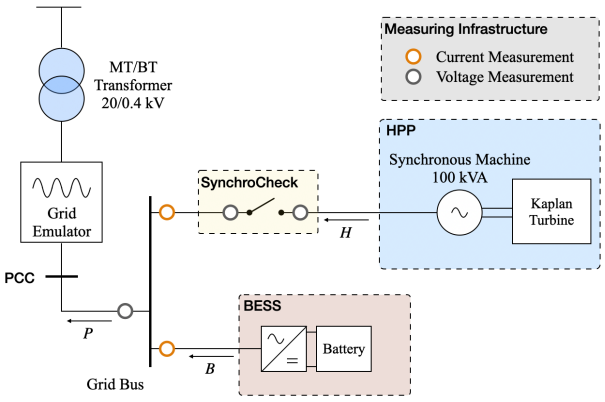

Fig. 4. Schematics of the PTMH PF3 power grid used to carry out the experiments

is illustrated in Fig. 5. This frequency data corresponds to measurements taken on January 8th, 2021, when the ENTSO continental Europe synchronous area experienced a system split. This particular time frame is chosen to ensure the inclusion of typical daily frequency patterns, for the first 8 hours of test, and also to subject the system to more challenging scenarios in the remaining 4 hours. More information about the system split event can be found in [25]. Under the described grid conditions, the following tests are conducted:

a) Kaplan unit operating alone.
b) Hybrid Kaplan unit with a 5 kW/5 kW h BESS, controlled by a *Dead Band Filter* (DBF) .
c) Hybrid Kaplan unit with a 9 kW/9 kW h BESS, controlled by DBF.
d) Hybrid Kaplan unit with a 5 kW/5 kW h BESS, controlled by DLMPC.
e) Hybrid Kaplan unit with a 9 kW/9 kW h BESS, controlled by DLMPC.

The DBF control strategy involves applying a dead-band filter to the frequency signal input of the governor, analogous to the approach described in [7]. Under this control scheme, frequency deviations below the threshold associated with the

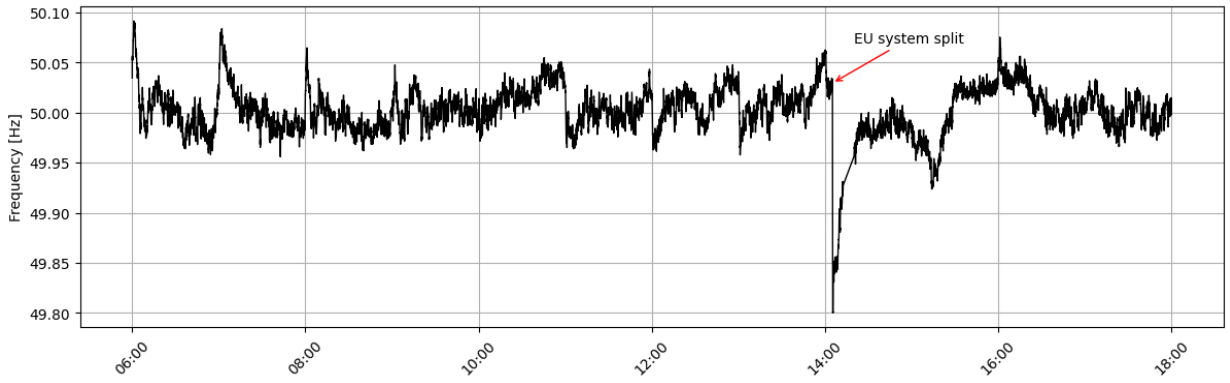

Fig. 5. Frequency Time Series for the test. Measurement from SwissGrid during the system split of the 8th of January 2021 [25]

BESS's maximum power capacity are managed by the BESS, whereas deviations exceeding this threshold are handled by the hydroelectric unit. For example, with a 5 kW BESS, the frequency threshold for DBF control is set at 40 mHz, and for a 9 kW BESS, it is 72 mHz. For detailed information on BESS sizing and the determination of these thresholds, see Appendix B. Unlike the method in [7], the DBF control strategy incorporates an upper layer to act as an SOE manager for the BESS. Thus, the difference between cases b) and d) lies in the application of DBF on the frequency input of the governor in the former, while the latter employs real-time solving of Problem (12). All the tests are performed considering a flat dispatch plan of 27 kW, constant for the 12 hours, to ensure that the wear and tear analysis of the movements is only related to FCR support. Moreover, the head of the system is kept constant at 10 m.

As for the DLMPC approach, the ULMPC is executed hourly based on the energy prediction for regulation, as outlined in Appendix A. On the other hand, the LLMPC runs every second using a sliding window spanning 30 seconds. Additional information about short-term frequency forecasting is also detailed in Appendix A.

C. Results

This analysis aims to highlight the advantages of BESS hybridization and to conduct a comparative assessment of distinct control techniques across various *Key Performance Indicators* (KPIs). This comprehensive analysis covers three primary aspects: the quality of the FCR provision, the mitigation of wear and tear on the hydroelectric governing system, and the safe operation of the BESS.

1) FCR provision quality: To assess the effectiveness of the FCR provision, we introduce the *Root Mean Squared* (RMS) of the tracking error TE, as defined in Eq. (6), computed over the full experiment time horizon. By integrating over a certain amount of time Δt the power error it is possible to estimate a mean energy error $E_k^{k+\Delta t}$, as follows:

$$E_k^{k+\Delta t} = \frac{1}{\Delta t} \sum_{k}^{k+\Delta t} \mathrm{TE}_k \tag{13}$$

The RMS values of the energy error, computed for $\Delta t = 30\,\mathrm{s}$, are presented in Table II. The selection of a 30 s interval aligns with FCR requirements from the grid code, which mandate that 100% of the FCR capacity has to be activated within 30 seconds [26]. Although the BESS size contributes

Configuration	Error (30s)
DBF (5 kW/5 kW h BESS)	0.3872 (−47.18%)
DBF (9 kW/9 kW h BESS)	0.3544 (−51.65%)
DLMPC (5 kW/5 kW h BESS)	0.3696 (−49.58%)
DLMPC (9 kW/9 kW h BESS)	0.3468 (−52.69%)
Only Hydro	0.7331 (+ 0.00%)

TABLE II
RMSE VALUES AND REDUCTION (%) OF THE TRACKING ERROR (TE) WITH RESPECT TO *Only Hydro*.

to reducing the RMS of TE, the impact is not notably significant. Interestingly, the DBF and DLMPC techniques can be considered equivalent in terms of set point tracking quality. Nonetheless, for data aggregated at 30-second intervals, the tracking error of any hybrid system demonstrates a reduction of at least 50% in comparison to the error exhibited by the non-hybrid system. Overall, the presence of a BESS alongside the HPP, regardless of the control strategy employed, enhances the system's responsiveness and improves its ability to accurately track the FCR service.

2) Wear and Tear Reduction: The assessment of wear reduction benefits is undertaken through the consideration of three specific KPIs: servomotors mileage, *Number of Movements* (NoM) and torque oscillation on the blades. The reduction in both guide vane and runner blade NoM and mileage are significant indicators of the wear reduction achieved through hybridization [6]. Table III provides a comprehensive overview of this wear reduction, underscoring the substantial advantages offered by the MPC technique. All the percentage values are computed relative to the baseline configuration, represented by 'Only Hydro'. Notably, the DLMPC control method demonstrates superior performance compared to the DBF control. The degree of improvement achieved through more sophisticated control techniques is particularly pronounced for smaller BESS sizes. In essence, when the BESS size is

sufficiently large, the necessity for optimal control diminishes. For instance, in the 5 kW BESS experiments, the DBF control attains a substantial reduction of 90.7% in runner blade mileage and 91.6% in the number of movements. Similarly, with the same BESS size, the DLMPC algorithm demonstrates even greater reductions, achieving 94.0% and 97.1% reduction in runner blade angle mileage and the number of movements, respectively. Comparable outcomes are observed when examining the corresponding reduction in guide vane servomotors. These findings highlight the benefits of implementing hybridization with advanced control techniques such as DLMPC, particularly standing out for its wear reduction performance for smaller BESS sizes. Finally, for an estimate of the forces that affect the blades and their servomechanisms, the torque oscillations occurring on the runner blades are evaluated. As outlined in [27], strain gauge testing emerges as the sole reliable approach for acquiring both static and dynamic stress information from the runner. Over recent years, this method has gained widespread acceptance as a standard practice for newly installed runners, as highlighted in [28]. To capture torque data, strain gauges are employed on the runner blades. The torque values recorded from 14:00 to 15:00, immediately following the system split, are depicted in the first three subplots of Figure RBT (Fig. 6). These graphs offer insights into the performance across various configurations. The uppermost subplot focuses on the scenario where the Kaplan turbine is the sole FCR provider. Here, the torque on the turbine blades exhibits continuous oscillations, which can be attributed to servomotor movements and consequent fluctuating flow/discharge conditions.

In the second subplot, we compare the behavior of the DBF-controlled 5 kW BESS hybrid system and the DLMPC-controlled 5 kW BESS hybrid system. Initially, both systems demonstrate parallel behavior up until 14:10. At this point, a significant frequency deviation occurs, leading to the saturation of BESS action in the DBF system. Consequently, from 14:10 to 14:22, the HPP is primarily responsible for regulation, as indicated by the noticeable torque oscillations during this interval. In contrast, the DLMPC system preemptively adapts the HPP power output to de-saturate the BESS, thereby maintaining its ability to provide rapid regulation. This adaptability underscores the fundamental difference between the simplistic DBF control strategy and the more sophisticated DLMPC approach. A similar trend is observable in the third subplot, which examines systems with larger BESS capacities. However, it is important to note that the benefits of a more advanced control strategy are less pronounced with larger BESS sizes. Overall, the time-domain subplots (the first three from the top) in Fig. 6 demonstrate that incorporating any BESS-hybrid system, regardless of its size, substantially reduces torque oscillations on the turbine blades compared to the 'Only Hydro' configuration.

To obtain a comprehensive analysis of torque oscillation reduction over the experiment duration, the *Cumulative Density Function* (CDF) of the blade torque derivative is further examined in the last subplot of Fig. 6. In line with the trends observed in other wear reduction KPIs and with what is visible in the time-domain subplots, the sole hydro case demonstrated inferior performance, characterized by elevated levels of torque oscillations on the blades. In the case of the 5 kW BESS, it is noticeable that the CDF of the blade torque derivative is significantly narrower under the DLMPC control strategy compared to DBF. This narrower distribution implies that there are fewer occurrences of high torque oscillations, indicating improved performance in mitigating such oscillations with DLMPC. The presence of a larger BESS size demonstrates a positive impact on the torque oscillation reduction. The *'Only Hydro'* scenario emerges as the least effective, marked by higher torque oscillations, thus underperforming in comparison to other configurations.

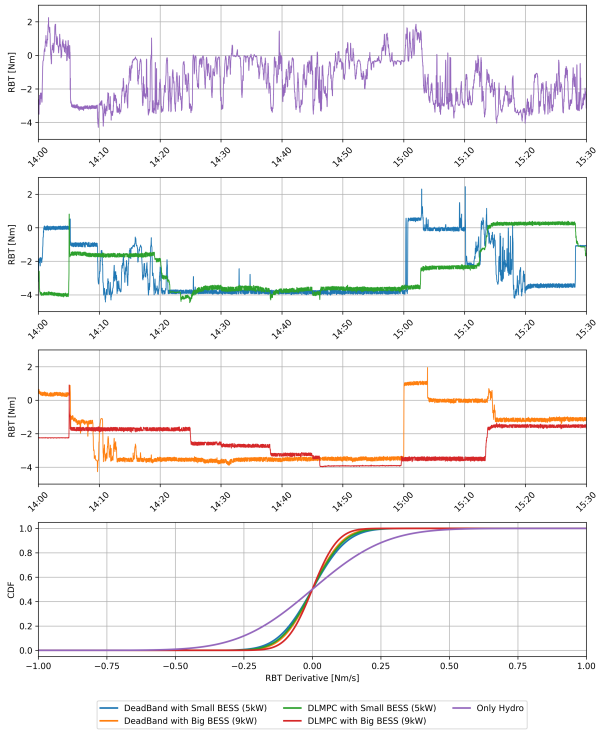

Fig. 6. Comparative analysis of Blade Torque Oscillation for the different scenarios.

3) Safe BESS Operation: The BESS SOE evolution over the 12 hours, for each experiment, is illustrated in Fig. 7. It is worth noting that, the two DBF experiments operate effectively until the grid split event occurs, around 14h00. Indeed, the regulating energy prediction from Eq. (14), is designed to function correctly in approximately 95% of cases (see Table IV) under normal grid conditions. However, in the event of a grid disruption, the power grid dynamics drastically change, and the new grid configuration differs from the one on which the SARIMA model was originally trained. Consequently, both DBF control strategies are unable to control the SOE within its limits during the latter half of the experiment. In contrast, the DLMPC strategy continually monitors the BESS SOE by means of the LLMPC. This frequent monitoring guarantees that the BESS operates within its predefined operational limits,

TABLE III
REDUCTION IN MILEAGE AND MOVEMENTS (%)

Configuration	Guide Vanes Opening (GVO)		Runner Blade Angle (RBA)	
	Mileage	Number of Movements	Mileage	Number of Movements
DBF (5 kW BESS)	4.18 (-91.5%)	662 (-92.9%)	3.06 (-90.7%)	753 (-91.6%)
DBF (9 kW BESS)	0.98 (-98.0%)	126 (-98.6%)	0.70 (-97.9%)	128 (-98.6%)
DLMPC (5 kW BESS)	3.33 (-93.2%)	292 (-96.8%)	1.98 (-94.0%)	258 (-97.1%)
DLMPC (9 kW BESS)	0.99 (-98.0%)	64 (-99.3%)	0.61 (-98.2%)	52 (-99.4%)
Only Hydro	49.03 (+0.00%)	9261 (+0.00%)	32.93 (+0.00%)	8970 (+0.00%)

even if the FCR energy prediction E_{FCR} deviates from the expected values. This feature substantially bolsters the system's reliability, allowing it to adapt to unforeseen grid dynamics.

V. CONCLUSION

In this paper, we present a comprehensive solution to address operational challenges in Run-of-River Hydropower Plants (RoR HPPs) related to continuous power regulations due to Frequency Containment Reserve (FCR) provision. By integrating Battery Energy Storage Systems (BESS) with RoR HPPs using a double-layer Model Predictive Control (MPC) approach, we validate a novel strategy to enhance FCR capabilities and simultaneously reduce wear and tear. The proposed control framework consists of an upper layer MPC responsible for State-of-Charge management of the BESS and a lower layer MPC for the optimal splitting policy of power set points between the turbine and the BESS. Rigorous reduced-scale experiments conducted in an innovative testing platform validated the effectiveness of the proposed MPC-based control strategy across diverse grid scenarios and BESS sizing. The experimental results showcased the superiority of the double-layer MPC strategy over simpler techniques such as dead-band control. The hybridized system showcased enhanced FCR provision quality and a notable reduction in servomechanism stress. The analysis of wear reduction revealed a substantial decrease in both guide vane and runner blade angle mileage, ranging from 93.2% with a 5 kW BESS to as much as 98% for a 9 kW BESS. Similar reductions were observed in the case of movements. Moreover, reduced torque oscillations on the blades further emphasize the benefits of the proposed hybridization approach. Future work on the subject involves an experimental comparison between the hybridization scenario outlined and the implementation of variable speed for the Kaplan turbine used as a propeller, i.e. with fixed blades.

REFERENCES

[1] B. Hase and C. Seidel, "Balancing services by run-of-river-hydropower at low reservoir amplitudes: Potentials, revenues and emission impacts," *Applied Energy*, vol. 294, p. 116988, Jul. 2021. [Online]. Available: https://linkinghub.elsevier.com/retrieve/pii/S0306261921004578

[2] ENTSOE, "Statistical Factsheet 2022," European Network of Transmission System Operators, Tech. Rep., 2022. [Online]. Available: https://eepublicdownloads.blob.core.windows.net/public-cdn-container/clean-documents/Publications/Statistics/Factsheet/entsoe_sfs2022_web.pdf

[3] W. Yang, P. Norrlund, L. Saarinen, A. Witt, B. Smith, J. Yang, and U. Lundin, "Burden on hydropower units for short-term balancing of renewable power systems," *Nature Communications*, vol. 9, no. 1, p. 2633, Dec. 2018. [Online]. Available: http://www.nature.com/articles/s41467-018-05060-4

[4] D. Valentín, A. Presas, M. Egusquiza, and C. Valero, "Hybridization in Kaplan turbines. Wear and tear assessment," *IOP Conference Series: Earth and Environmental Science*, vol. 1079, no. 1, p. 012108, Sep. 2022. [Online]. Available: https://iopscience.iop.org/article/10.1088/1755-1315/1079/1/012108

[5] T. Makinen, A. Leinonen, and M. Ovaskainen, "Modelling and benefits of combined operation of hydropower unit and battery energy storage system on grid primary frequency control," in *2020 IEEE International Conference on Environment and Electrical Engineering and 2020 IEEE Industrial and Commercial Power Systems Europe (EEEIC / I&CPS Europe)*. Madrid, Spain: IEEE, Jun. 2020, pp. 1–6. [Online]. Available: https://ieeexplore.ieee.org/document/9160666/

[6] D. Valentín, A. Presas, M. Egusquiza, J.-L. Drommi, and C. Valero, "Benefits of battery hybridization in hydraulic turbines. Wear and tear evaluation in a Kaplan prototype," *Renewable Energy*, vol. 199, pp. 35–43, Nov. 2022. [Online]. Available: https://linkinghub.elsevier.com/retrieve/pii/S0960148122012927

[7] S. Kadam, W. Hofbauer, S. Lais, M. Neuhauser, E. Wurm, L. F. Lameiro, Y.-M. Bourien, G. Païs, J.-L. Drommi, C. Nicolet, C. Landry, M. Dreyer, C. Valero, A. Presas, and D. Valentin, "Hybridization of a RoR HPP with a BESS—The XFLEX HYDRO Vogelgrun Demonstrator," *Energies*, vol. 16, no. 13, p. 5074, Jun. 2023. [Online]. Available: https://www.mdpi.com/1996-1073/16/13/5074

[8] S. Cassano and F. Sossan, "Model predictive control for a medium-head hydropower plant hybridized with battery energy storage to reduce penstock fatigue," *Electric Power Systems Research*, vol. 213, p. 108545, Dec. 2022. [Online]. Available: https://linkinghub.elsevier.com/retrieve/pii/S0378779622006484

[9] F. Gerini, E. Vagnoni, M. Seydoux, R. Cherkaoui, and M. Paolone, "Experimental facility for reduced scale model testing of hydraulic machines hybridized with a battery energy storage system," *IOP Conference Series: Earth and Environmental Science*, vol. 774, no. 1, p. 012119, Jun. 2021. [Online]. Available: https://iopscience.iop.org/article/10.1088/1755-1315/774/1/012119

[10] ENTSOE, "TSOs' proposal for the establishment of common and harmonised rules and pro- cesses for the exchange and procurement of Balancing Capacity for Frequency Containment Reserves (FCR) in accordance with Article 33 of Commission Regulation (EU) 2017/2195 establishing a guideline on elec- tricity balancing," 2018. [Online]. Available: https://eepublicdownloads.blob.core.windows.net/public-cdn-container/clean-documents/Network%20codes%20documents/NC%20EB/FCR_Proposal-Article_33_1%20EBGL_20181018_FV.PDF

[11] ——, "All CE TSOs' proposal for additional properties of FCR in accordance with Article 154(2) of the Commission Regulation (EU) 2017/1485 of 2 August 2017 establishing a guideline on electricity transmission system operation," 2019. [Online]. Available: https://eepublicdownloads.entsoe.eu/clean-documents/nc-tasks/EBGL/SOGL_A118_A154(2)_190322_Additional%20Properties%20of%20FCR_All%20TSO%27s%20CE_final%20submission_Explanatory%20Note.pdf

[12] S. Ltd, "Conditions for prequalification (primary, secondary and tertiary control, in German) - Präqualifikationsbedingungen," 2009. [Online]. Available: https:

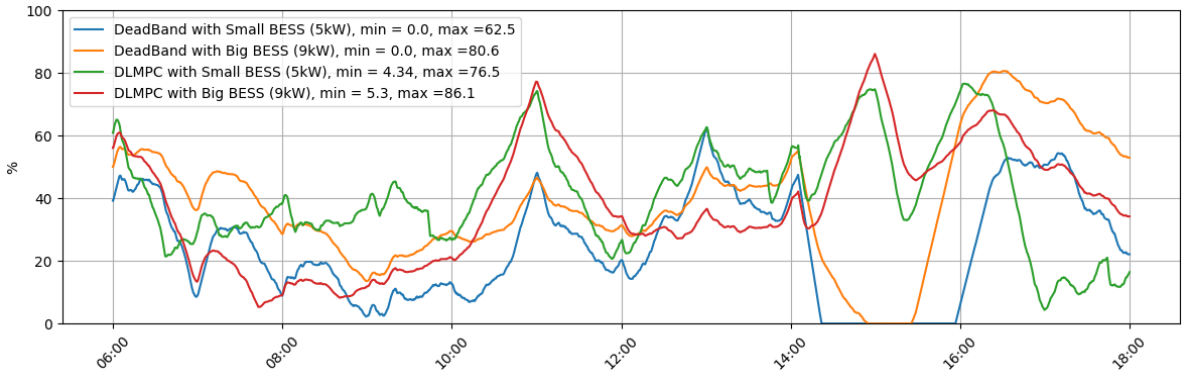

Fig. 7. BESS SOE evolution during the different experiments

//www.swissgrid.ch/dam/swissgrid/customers/topics/ancillary-services/prequalification/2/Anhang-01-Praequalifikationsbedingungen-de.pdf

[13] G. Piero Schiapparelli, S. Massucco, E. Namor, F. Sossan, R. Cherkaoui, and M. Paolone, "Quantification of Primary Frequency Control Provision from Battery Energy Storage Systems Connected to Active Distribution Networks," in *2018 Power Systems Computation Conference (PSCC)*. Dublin: IEEE, Jun. 2018, pp. 1–7. [Online]. Available: https://ieeexplore.ieee.org/document/8442554/

[14] F. Gerini, E. Vagnoni, R. Cherkaoui, and M. Paolone, "Improving frequency containment reserve provision in run-of-river hydropower plants," *Sustainable Energy, Grids and Networks*, vol. 28, p. 100538, Dec. 2021. [Online]. Available: https://linkinghub.elsevier.com/retrieve/pii/S2352467721001090

[15] P. Haessig, "Convex Storage Loss Modeling for Optimal Energy Management," in *2021 IEEE Madrid PowerTech*. Madrid, Spain: IEEE, Jun. 2021, pp. 1–6. [Online]. Available: https://ieeexplore.ieee.org/document/9494786/

[16] S. P. Boyd and L. Vandenberghe, *Convex optimization*. Cambridge, UK ; New York: Cambridge University Press, 2004.

[17] F. Gerini, Y. Zuo, R. Gupta, A. Zecchino, Z. Yuan, E. Vagnoni, R. Cherkaoui, and M. Paolone, "Optimal grid-forming control of battery energy storage systems providing multiple services: Modeling and experimental validation," *Electric Power Systems Research*, vol. 212, p. 108567, Nov. 2022. [Online]. Available: https://linkinghub.elsevier.com/retrieve/pii/S0378779622006496

[18] F. Sossan, E. Namor, R. Cherkaoui, and M. Paolone, "Achieving the Dispatchability of Distribution Feeders Through Prosumers Data Driven Forecasting and Model Predictive Control of Electrochemical Storage," *IEEE Transactions on Sustainable Energy*, Oct. 2016.

[19] M. Bahramipanah, D. Torregrossa, R. Cherkaoui, and M. Paolone, "Enhanced electrical model of Lithium-based batteries accounting the charge redistribution effect," in *2014 Power Systems Computation Conference*. Wrocław, Poland: IEEE, Aug. 2014, pp. 1–8. [Online]. Available: http://ieeexplore.ieee.org/document/7038481/

[20] A. Zecchino, Z. Yuan, F. Sossan, R. Cherkaoui, and M. Paolone, "Optimal provision of concurrent primary frequency and local voltage control from a BESS considering variable capability curves: Modelling and experimental assessment," *Electric Power Systems Research*, vol. 190, p. 106643, Jan. 2021.

[21] A. Borghetti, M. D. Silvestro, G. Naldi, M. Paolone, and M. Alberti, "Maximum Efficiency Point Tracking for Adjustable-Speed Small Hydro Power Plant," in *2008 Power Systems Computation Conference (PSCC)*. IEEE, 2008, p. 7.

[22] I. a. o. Standard, "IEC 60193:2019 Hydraulic turbines, storage pumps and pump-turbines—model acceptance tests," *International Electrotechnical Commission,*, 2019. [Online]. Available: https://webstore.iec.ch/publication/60951

[23] P. Kundur, "Power System Stability," in *Power System Stability and Control*, L. Grigsby, Ed. CRC Press, May 2007, vol. 20073061, series Title: Electrical Engineering Handbook. [Online]. Available: http://www.crcnetbase.com/doi/abs/10.1201/9781420009248.sec2

[24] P. Romano and M. Paolone, "Enhanced Interpolated-DFT for Synchrophasor Estimation in FPGAs: Theory, Implementation, and Validation of a PMU Prototype," *IEEE Transactions on Instrumentation and Measurement*, vol. 63, no. 12, pp. 2824–2836, Dec. 2014. [Online]. Available: http://ieeexplore.ieee.org/document/6818415/

[25] E. ICS Investigation Expert Panel, "Continental Europe Synchronous Area Separation on 08 January 2021 - Final Report," ENTSO-E, Tech. Rep., Jul. 2021. [Online]. Available: https://eepublicdownloads.azureedge.net/clean-documents/SOC%20documents/SOC%20Reports/entso-e_CESysSep_Final_Report_210715.pdf

[26] P. Maucher and H. Lens, "On the specification of requirements for the activation dynamics of Frequency Containment Reserves," in *2021 IEEE International Conference on Communications, Control, and Computing Technologies for Smart Grids (SmartGridComm)*. Aachen, Germany: IEEE, Oct. 2021, pp. 45–50. [Online]. Available: https://ieeexplore.ieee.org/document/9632295/

[27] A. Presas, D. Valentin, W. Zhao, M. Egusquiza, C. Valero, and E. Egusquiza, "On the use of neural networks for dynamic stress prediction in Francis turbines by means of stationary sensors," *Renewable Energy*, vol. 170, pp. 652–660, Jun. 2021. [Online]. Available: https://linkinghub.elsevier.com/retrieve/pii/S0960148121001804

[28] A. Presas, Y. Luo, Z. Wang, and B. Guo, "Fatigue life estimation of Francis turbines based on experimental strain measurements: Review of the actual data and future trends," *Renewable and Sustainable Energy Reviews*, vol. 102, pp. 96–110, Mar. 2019. [Online]. Available: https://linkinghub.elsevier.com/retrieve/pii/S1364032118307974

[29] L. Zanni, A. Derviškadić, M. Pignati, C. Xu, P. Romano, R. Cherkaoui, A. Abur, and M. Paolone, "PMU-based linear state estimation of Lausanne subtransmission network: Experimental validation," *Electric Power Systems Research*, vol. 189, p. 106649, Dec. 2020. [Online]. Available: https://linkinghub.elsevier.com/retrieve/pii/S0378779620304521

[30] N. Chettibi, A. Massi Pavan, A. Mellit, A. Forsyth, and R. Todd, "Real-time prediction of grid voltage and frequency using artificial neural networks: An experimental validation," *Sustainable Energy, Grids and Networks*, vol. 27, p. 100502, Sep. 2021. [Online]. Available: https://linkinghub.elsevier.com/retrieve/pii/S2352467721000734

[31] NGESO, "Historic Frequency Data," 2019. [Online]. Available: https://data.nationalgrideso.com/system/system-frequency-data?from=40#resources

[32] H. Hesse, M. Schimpe, D. Kucevic, and A. Jossen, "Lithium-Ion Battery Storage for the Grid—A Review of Stationary Battery Storage System Design Tailored for Applications in Modern Power Grids," *Energies*, vol. 10, no. 12, p. 2107, Dec. 2017. [Online]. Available: https://www.mdpi.com/1996-1073/10/12/2107

APPENDIX A
FREQUENCY FORECASTING

A. Regulating Energy Forecasting

Both the upper-layer and lower-layer MPC rely on distinct types of frequency forecasting. In the upper layer MPC, a forecast of the FCR regulating energy for the next hour is necessary. This entails estimating the integral of the frequency deviation over time, once the droop is defined. The ability to predict this quantity was initially introduced in [13] and subsequently adopted by various researchers, including [14]. In this contribution, we propose an enhanced model for frequency forecasting and compare its performance with the model from [13] in terms of standard deviation. The formulation for FCR energy estimation during an hour g is given by:

$$E_{\text{FCR}} = \int_g P_{\text{FCR}} dt = \int_g \sigma_f \cdot \Delta f dt = \sigma_f W_g, \qquad (14)$$

where σ_f is the frequency droop. The motivation for updating the models stems from a more comprehensive statistical analysis carried out by the authors using a one-year-long set of frequency time series (from March 2019 to April 2020). This analysis clearly demonstrates a discernible seasonality effect on a daily basis, as evident from Fig. 8, which was not considered in the model of [13]. For this reason, a new *Seasonal Auto Regressive Integrated Moving Average* (SARIMA) model is introduced. We present the model and its performance over a testing set of data (from September 2020 to December 2020) in Table IV. In this table, γ_T indicates the time intervals at which the residuals exceed the corresponding 95% or 99% confidence intervals. It is defined as follows:

$$\gamma_T = \frac{\text{Time with } |r_i| \geq k\sigma}{\text{Total observation time}}, \qquad (15)$$

where σ represents the variance and k takes values 2 and 3 for the 95% and 99% intervals, respectively.

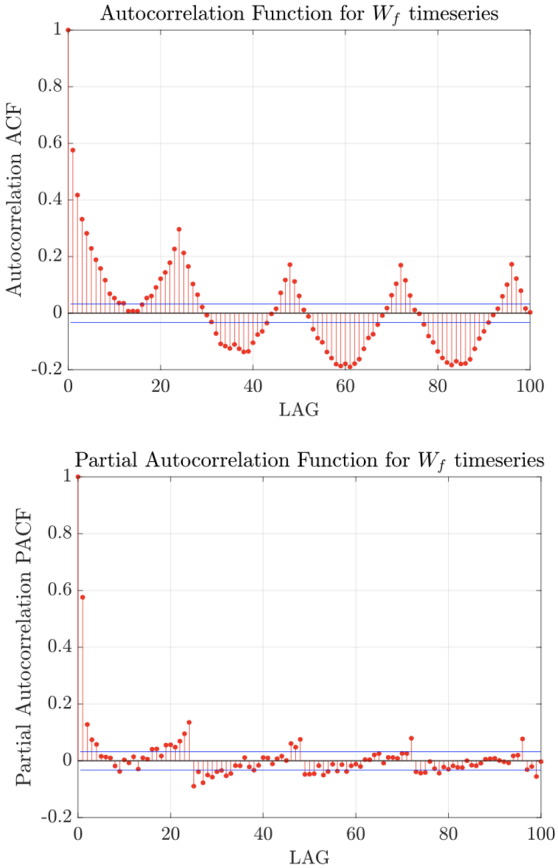

Fig. 8. W_g Auto-Correlation Function (ACF) above and Partial Auto-Correlation Function (PACF) below.

Models	σ	ρ	γ_T	MSE
ARIMA$(8,0,0)(0,0,0)$	25	95%	7.2%	562
	25	99%	1.5%	562
SARIMA$(6,0,0)(0,1,1)_{24}$	22	95%	7.2%	485
	22	99%	2.1%	485
Dataset: PMU-5, EPFL, September 2020 - December 2020 [29]				

TABLE IV
COMPARISON BETWEEN THE FORECASTING MODEL USED IN THE UPPER LAYER MPC AND [13].

Lastly, a residual analysis of the SARIMA model is conducted, to demonstrate that the proposed model cannot be further improved by increasing the order of the model. The residuals exhibit a zero-mean normal distribution. Furthermore, a Durbin-Watson test confirms the absence of correlation among the residuals. The test statistic is computed as:

$$s = \frac{\sum_{i=2}^{N} (r_i - r_{i-1})^2}{\sum_{i=1}^{N} (r_i)^2} = 2.0051.$$

Given its enhanced performance, the forecaster selected to produce the regulating energy prediction fed to the upper layer MPC during the experimental validation is SARIMA$(6,0,0)(0,1,1)_{24}$. This specification denotes an AR model of order 6, coupled with a seasonal component that has no seasonal AR effects, one order of seasonal differencing, and a seasonal MA component of order 1 with a seasonality of 24 h.

B. Short-Term Frequency Forecasting

Frequency prediction is a crucial component of the lower-layer MPC. Specifically, the experimental validation that employs the lower layer MPC necessitates second-interval predictions for a 30-second horizon. The inherent stochastic behavior of grid frequency in bulk power systems poses a significant challenge in achieving accurate predictions. In fact, only a limited number of studies have explored the feasibility of such predictions. One exception can be found in [30], which introduces the real-time prediction of grid voltage and frequency using artificial neural networks. This method primarily focuses on short-term frequency prediction (0.183 ms and 1 sec), demonstrating satisfactory *Root Mean Squared Error* (RMSE) values for both one-step and three-step ahead predictions. However, the RMSE achieved through this

approach is on par with the RMSE obtained from a simple AR(0) regression model. This regression model essentially assumes continuity, implying that the subsequent frequency measurement remains consistent with the preceding one. In details, [30] claims an RMSE$= 0.0039$ Hz of their one-sec ahead forecaster tested for during one day of May 2019. AR(0) regression model for secondly-sampled frequency timeseries for the same month (data from: [31]) results in an RMSE $= 0.0024$. However, given that the data-set utilized in [30] is not publicly accessible, offering more comprehensive insights presents a challenge. Consequently, the frequency predictor for the lower-layer MPC does not hinge on genuine forecasting, but rather assumes that the forthcoming 30 seconds of frequency will mirror the preceding values.

APPENDIX B
BESS SIZING FOR EXPERIMENTAL VALIDATION

Optimal BESS sizing for this application is beyond the scope of this study, as it requires comprehensive consideration of various factors and extended time frames. However, the authors wish to clarify the rationale behind the BESS sizing during for the experimental campaign.

As delineated in [4], the hydro-turbine governor at Vogelgrun Hydropower Plant (HPP) is characterized by a regulating energy of $4\,\mathrm{MW}$ (11.5% of its nominal power) for a $200\,\mathrm{mHz}$ frequency deviation, i.e. a droop of $20\,\mathrm{MW\,Hz^{-1}}$. Scaling this to the tested reduced-scale model yields a $28.75\,\mathrm{kW\,Hz^{-1}}$ droop with $5.75\,\mathrm{kW}$ of regulating power at $200\,\mathrm{mHz}$ deviation. However, this regulating power isn't feasible due to battery size constraints and potential interference with power oscillation noise.

To address the latter problem, the facility's droop is increased to $125\,\mathrm{kW\,Hz^{-1}}$. In accordance with [4], the installed BESS at Vogelgrun constitutes 16.5% of the regulating energy, equivalent to $4.125\,\mathrm{kW}$. For experimentation, we opted for two BESS sizes: $5\,\mathrm{kW}$ and $9\,\mathrm{kW}$. The BESS power rating is the consequence of a statistical analysis of frequency timeseries in the continental Europe power system, aiming to cover 95% and 99% of frequency deviations. Figure 9 offers a visual representation of the CDF of frequency deviation in the ENTSO synchronous area, together with the power ratings derived by assuming a droop of $125\,\mathrm{kW\,Hz^{-1}}$. Regarding the BESS energy sizing, it is important to note that this assumption impacts the outcomes of the DLMPC. Specifically, a BESS with more energy capacity would necessitate fewer interventions from the DLMPC, whereas a BESS with lower energy capacity would require more frequent actions. Due to the complexity of the tests, we did not conduct experiments with varying energy ratings for each BESS power rating. Instead, we made the assumption of a power-to-energy ratio of 1, aligning with market availability as mentioned in [32]. Such an assumption is possible since the scope of the paper is not to provide optimal sizing, but rather to validate the control framework. Finally, during testing, as the BESS's capacity and power were software-limited, the converter's capability curve was not constrained by physical limits. Consequently, Eq. (10) was simplified to $B^{\mathrm{dch}}_{\max} \leq B_k \leq B^{\mathrm{ch}}_{\max}$. Future studies will focus on evaluating the optimal BESS sizing for addressing challenges related to BESS hybridization in HPPs.

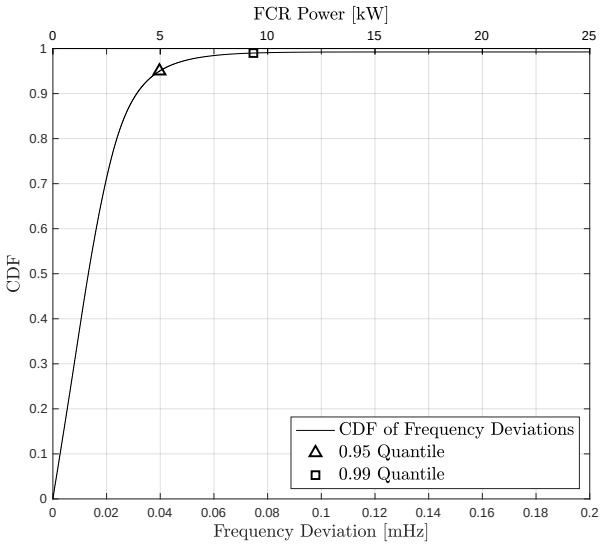

Fig. 9. CDF of Frequency deviation in continental Europe, based on year-long time series collected between 2019 and 2020. On the upper x-axis the FCR power associated with the frequency deviation.